Plant Physiology and Biochemistry 143 (2019) 109–118

Contents lists available at ScienceDirect

Plant Physiology and Biochemistry

journal homepage: www.elsevier.com/locate/plaphy

Research article

LED lamps enhance somatic embryo maturation in association with the differential accumulation of proteins in the *Carica papaya* L. 'Golden' embryogenic callus

Felipe Astolpho Almeida[a,b], Ellen Moura Vale[a,b], Ricardo Souza Reis[a,b], Claudete Santa-Catarina[c], Vanildo Silveira[a,b,*]

[a] Laboratório de Biotecnologia, Centro de Biociências e Biotecnologia (CBB), Universidade Estadual Do Norte Fluminense Darcy Ribeiro (UENF), Campos Dos Goytacazes, RJ, 28013-602, Brazil
[b] Unidade de Biologia Integrativa, Setor de Genômica e Proteômica, UENF, Campos Dos Goytacazes, RJ, 28013-602, Brazil
[c] Laboratório de Biologia Celular e Tecidual, CBB, UENF, Campos Dos Goytacazes, RJ, Brazil

ARTICLE INFO

Keywords:
Carica papaya L.
Clonal propagation
Comparative proteomics
LED
Label-free proteomics
Light-emitting diode
Somatic embryogenesis

ABSTRACT

The use of light-emitting diode (LED) lamps has been shown to be a promising approach for improving somatic embryo maturation during somatic embryogenesis. The aim of this work was to study the influence of the light source on somatic embryo differentiation and its relationship with the differential abundance of proteins in the *Carica papaya* L. 'Golden' embryogenic callus at 14 days of maturation. The white plus medium-blue (W_mB) LED and fluorescent lamp treatments produced an average of 82.4 and 47.6 cotyledonary somatic embryos per callus, respectively. A shotgun proteomics analysis revealed 28 upaccumulated and 7 downaccumulated proteins. The proteins upaccumulated in the embryogenic callus matured under the W_mB LED lamp compared with that matured under the fluorescent lamp included indole-3-acetic acid-amido synthetase (GH3) and actin-depolymerizing factor 2 (ADF2), which are involved in the regulation of auxin levels by auxin conjugation and transport. Additionally, proteins related to energy production (aconitate, ADH1, GAPCp, PKp and TPI), cell wall remodeling (PG and GLPs), and intracellular trafficking (NUP50A, IST1, small GTPases and H^+-PPase) showed significantly higher abundance in the embryogenic callus incubated under the W_mB LED lamp than in that incubated under the fluorescent lamp. The results showed that the W_mB LED lamp improved somatic embryo maturation in association with the differential accumulation of proteins in the *C. papaya* 'Golden' embryogenic callus.

1. Introduction

Papaya (*Carica papaya* L.), an important perennial fruit tree distributed in the tropical and subtropical regions of the world, has high amounts of vitamins and minerals and is used in the food, pharmacological, and textile industries (Dhekney et al., 2016). The fruits of this cultivar have been accepted in the European and North American markets due to their flavor and pulp qualities. In addition, these fruits are a rich source of bioactive compounds such as carotenoids (Fabi et al., 2007). Commercially, *C. papaya* propagation is seminiferous, but this propagation method is limited by several factors, such as the heterogeneity of cross-pollination (Bhattacharya and Khuspe, 2001).

Micropropagation by somatic embryogenesis is a potential alternative to seminiferous propagation. This biotechnological approach enables the large-scale clonal production of disease-free plants with genetic value and provides suitable targets for genetic transformation (Heringer et al., 2018). Furthermore, the developmental stages of the somatic embryogenesis of *C. papaya*, including the globular, heart, torpedo and cotyledonary stages, are similar to those of zygotic embryogenesis in dicots (Vale et al., 2018), which demonstrates that somatic embryogenesis can potentially serve as an efficient experimental model for genetic, physiological and morphological studies of the formation and development of embryos in plants.

The induction of somatic embryogenesis requires stress treatment of an explant, such as exposure to synthetic auxins, which results in the dedifferentiation of somatic plant cells followed by the reacquisition of cellular totipotency (Fehér, 2015). Stress and exogenous hormones are involved in epigenetic modifications that control the dynamic

* Corresponding author. Laboratório de Biotecnologia, Centro de Biociências e Biotecnologia (CBB), Universidade Estadual do Norte Fluminense Darcy Ribeiro (UENF), Campos dos Goytacazes, RJ, 28013-602, Brazil.
E-mail address: vanildo@uenf.br (V. Silveira).

https://doi.org/10.1016/j.plaphy.2019.08.029
Received 27 February 2019; Received in revised form 28 August 2019; Accepted 29 August 2019
Available online 30 August 2019
0981-9428/

Abbreviations

2,4-D	2,4-dichlorophenoxyacetic acid
ADF	actin-depolymerizing factor
ADH	alcohol dehydrogenase
ANOVA	analysis of variance
CDC48	cell division cycle 48
CV	coefficient of variation
DIA	data-independent acquisition
DTT	dithiothreitol
FC	fold change
FDR	false discovery rate
FW	fresh weight
FWHM	full width at half maximum
H^+-PPase	proton-translocating inorganic pyrophosphatase
GABA	γ-aminobutyric acid
GAPCp	glyceraldehyde-3-phosphate dehydrogenase chloroplastic
GH3	IAA-amido synthetase
GLP	germin-like protein
IMS	ion mobility separation
LED	light-emitting diode
MS	Murashige and Skoog culture medium
MVB	multivesicular bodies
PEG	polyethylene glycol
PG	polygalacturonase
PKp	pyruvate kinase chloroplastic
PMSF	phenylmethylsulfonyl fluoride;
SNK	student–Newman–Keuls
TCA	tricarboxylic acid cycle
TFA	trifluoroacetic acid
TGN	*trans*-Golgi network
TOF	time-of-flight
TPI	triosephosphate isomerase
W_hB	white plus high-blue LED lamp;
W_mB	white plus medium-blue LED lamp;
W_lB_dR	white plus low-blue and deep-red LED lamp;
W_mB_dR	white plus medium-blue and deep-red LED lamp;
$W_lB_dR_fR$	white plus low-blue, deep-red and far-red LED lamp;
$W_mB_dR_fR$	white plus medium-blue, deep-red and far-red LED lamp.

expression of specific genes associated with the new development program modulating the switching of cell fate (Mahdavi-Darvari et al., 2015). Epigenetic reprogramming has been associated with significant changes in transcription profiles during somatic embryogenesis (Pasternak and Dudits, 2019).

Somatic embryo development can be influenced by several factors, such as the light spectrum, which plays a central role in plant morphogenesis (Gupta and Jatothu, 2013). Light is perceived by photoreceptors, which absorb different wavelengths and transduce the signals to regulate gene expression and plant development (Wang et al., 2018). Red and far-red light are detected by phytochromes, whereas blue light is mainly detected by cryptochromes (Wang et al., 2018). These photoreceptors trigger complex signal transduction to regulate nuclear- and plastid-encoded genes and thereby induce developmental responses, such as somatic embryo induction, shoot formation, rhizogenesis, and the differentiation of chloroplast and photosynthetic apparatus (Gupta and Jatothu, 2013). However, gene expression in response to light signals undergoes different levels of control until active protein is obtained. In addition to epigenetic modifications, light can control small noncoding RNAs (Sánchez-Retuerta et al., 2018) and promote intense alternative splicing in the transcriptome, which directly influences increases in proteome complexity (Cheng and Tu, 2018).

The use of light-emitting diode (LED) lamps is a promising approach for optimizing plant growth conditions, and this approach has been successfully used for the somatic embryogenesis of several species, such as *Dimocarpus longan* (Li et al., 2018), *Saccharum* spp. (sugarcane) (Heringer et al., 2017) and *Vitis vinifera* 'Chardonnay' (Tittmann et al., 2015). The embryogenic callus of *D. longan* treated with LEDs with blue wavelengths accumulates flavonoids through the regulation of target genes by the expression of various miRNAs (Li et al., 2018). In sugarcane somatic embryogenesis, LEDs with both red and blue wavelengths promote a higher abundance of methyltransferases that affect the methylation patterns of DNA and thus the pool of proteins (Heringer et al., 2017).

Proteomics approaches have the potential to provide a basis for understanding the role of proteins in the regulation of plant somatic embryogenesis (Heringer et al., 2018). However, few studies have associated proteomics with the effects of LED light use on somatic embryogenesis, particularly in *C. papaya*. Proteomics analysis could be a relevant approach for understanding these effects that has strong potential to yield innovative results that can improve our understanding of the physiological and molecular bases of cell competence acquisition during somatic embryogenesis (Heringer et al., 2018).

Using LED lamps with different wavelengths, the present work aimed to evaluate the influence of light source on somatic embryo development and its relationship with the differential abundance of proteins in the *C. papaya* 'Golden' embryogenic callus at 14 days of maturation.

2. Materials and methods

2.1. Plant materials and induction of embryogenic callus

Mature zygotic embryos were excised from 'Golden' *C. papaya* seeds and used as explants for embryogenic callus induction. The fruits were provided by the Agricultural Caliman Company S/A, Linhares, ES, Brazil (19°23′S and 40°4′W).

We performed callus induction according to Vale et al. (2018). Briefly, the explants were placed in Petri dishes (90 × 15 mm) containing MS culture medium (Murashige and Skoog, 1962) (Phytotechnology Lab, Shawnee Mission, KS, USA) supplemented with 30 g dm^{-3} sucrose (Vetec, São Paulo, SP, Brazil), 20 μM 2,4-dichlorophenoxyacetic acid (2,4-D; Sigma-Aldrich, St. Louis, MO, USA) and 2.0 g dm^{-3} Phytagel (Sigma-Aldrich). The pH of the culture medium was adjusted to 5.8, and the medium was autoclaved at 121 °C for 15 min. Callus induction was performed in the dark under controlled temperature (25 ± 1 °C) for 45 days. Prior to the initiation of maturation treatment, the induced embryogenic callus was subcultured three times at 21-day intervals under the same culture conditions.

2.2. Light source treatments during embryogenic callus maturation

The first experiment performed in this study was designed to evaluate the influence of all six GreenPower TLEDs (Koninklijke Philips Electronics NV, Netherlands) and fluorescent lamps on somatic embryo maturation (Supplementary Table S1). The experiment was conducted using a completely randomized design, with five biological replicates per treatment, and each replicate involved a Petri dish containing three calli (300 mg of FW each). The maturation culture medium consisted of MS supplemented with 0.55 mM myo-inositol (Merck Millipore, Darmstadt, Germany), 30 g dm^{-3} sucrose and 60 g dm^{-3} polyethylene glycol (PEG; Sigma-Aldrich). The Petri dishes with the embryogenic calli were maintained in a growth chamber at 25 ± 1 °C in the dark for 7 days. Subsequently, Petri dishes were maintained under a 16-h photoperiod at 25 ± 1 °C for 28 days using seven different light source

treatments (Supplementary Table S1). At 28 days of maturation, the increment in the FW of the callus and the number of cotyledonary somatic embryos formed per callus (300 mg of initial FW) were evaluated.

Based on the results of the first experiment, a second experiment was performed using the W_mB LED lamp treatment, which produced the highest number of cotyledonary somatic embryos at 28 days of maturation, and the treatment with the fluorescent lamp, which is the conventional lamp used for somatic embryo maturation. In the second experiment, we performed seven replicates of each treatment using the same maturation conditions from the first experiment. Samples of embryogenic calli (300 mg of FW) matured under the W_mB LED lamp and under the fluorescent lamp at 14 days of maturation were stored at −80 °C for proteomic analysis. Embryogenic calli samples, at 14 days of maturation, used for proteomic analysis were composed of embryogenic cells and a mixture of somatic embryos at different stages of development.

Additionally, samples of embryogenic calli were used to count the number of somatic embryos at each developmental stage (globular, heart, torpedo, and cotyledonary) at 14 and 28 days of maturation.

2.3. Protein extraction

For proteomic analyses, we collected callus from the second experiment of embryogenic callus maturation under the W_mB LED lamp and under the fluorescent lamp treatments, at 14 days of maturation. Three randomized biological replicates (300 mg of FW each) were used for protein extraction. The samples were pulverized using a mortar and pestle and liquid nitrogen and then macerated with extraction buffer containing 7 M urea (GE Healthcare, Little Chalfont, UK), 2 M thiourea (GE Healthcare), 1% dithiothreitol (DTT; GE Healthcare), 1 mM phenylmethylsulfonyl fluoride (PMSF; Sigma-Aldrich), 2% Triton X-100 (GE Healthcare) and 5 μM pepstatin (Sigma-Aldrich). The samples were vortexed for 5 min, incubated on ice for 30 min, and centrifuged at 16,000 × *g* and 4 °C for 20 min, and the supernatants were collected. The total protein concentration was determined using a 2-D Quant Kit (GE Healthcare).

2.4. Protein digestion

The extracted proteins (100 μg from each biological replicate) were first precipitated with methanol chloroform for detergent removal according to Nanjo et al. (2012). Subsequently, the samples were resuspended in buffer containing 7 M urea and 2 M thiourea and desalted on Amicon Ultra 3-kDa centrifugal filters (Merck Millipore). Twenty-five microliters of 0.2% (v/v) RapiGest surfactant (Waters, Milford, MA, USA) was then added to each sample, and the resultant mixtures were briefly vortexed and incubated in an Eppendorf Thermomixer (Eppendorf, Hamburg, Germany) at 80 °C for 15 min. Afterward, 2.5 mm^3 of 100 mM DTT was added to each sample, and the resulting mixtures were incubated at 60 °C for 30 min. After the incubation, 2.5 mm^3 of 300 mM iodoacetamide (GE Healthcare) was added to each sample. The samples were incubated in the dark for 30 min at 25 °C, and 5 mm^3 of 100 mM DTT was then added to quench the excess iodoacetamide. Protein digestion was performed by adding 20 mm^3 of trypsin (50 ng mm^{-3}) (Promega, Madison, WI, USA) in 50 mM ammonium bicarbonate (Sigma-Aldrich) per sample followed by incubation for 15 h at 37 °C. Subsequently, 10 mm^3 of 5% (v/v) trifluoroacetic acid (TFA; Sigma-Aldrich) was added to each sample for RapiGest precipitation and trypsin activity inhibition; and the samples were then incubated at 37 °C for 30 min and centrifuged at 16,000 × *g* for 20 min. The peptide mixtures were transferred to total recovery vials (Waters) for direct use in a Synapt G2-Si mass spectrometer (Waters).

2.5. Analyses by mass spectrometry

Nano-LC-electrospray ionization (ESI)-MS/MS analysis was performed using a nanoAcquity UPLC (Waters) coupled to a Synapt G2-Si mass spectrometer (Waters). The peptide mixtures were separated by liquid chromatography by loading 1 μg of digested protein onto a nanoAcquity UPLC 5-μm C18 trap column (180 μm by 20 mm; Waters) followed by loading onto a nanoAcquity HSS T3 1.8-μm analytical column (75 μm by 150 mm; Waters) at a rate of 0.4 $mm^3\,min^{-1}$ and a temperature of 45 °C. The binary gradient used for peptide elution consisted of mass spectrometry-grade water (Tedia, Fairfield, OH, USA) and 0.1% formic acid (Sigma-Aldrich) as mobile phase A and acetonitrile (Tedia) and 0.1% formic acid as mobile phase B. The elution gradient was increased from 7% to 40% of solution B until 91.12 min, increased to 99.9% of solution B until 92.72 min, maintained at 99.9% of solution B until 106 min, decreased to 7% of solution B until 106.1 min, and then maintained at 7% of solution B until the run ended at 120 min.

Mass spectrometry was performed in the positive and resolution (V) modes, with a full width at half maximum (FWHM) of 35,000 and ion mobility, and in the data-independent acquisition (DIA) mode. The ion mobility separation (IMS) used an IMS wave velocity of 600 m s^{-1} ($HDMS^E$); the transfer collision energy was increased from 19 to 55 V in the high-energy mode; the cone and capillary voltages were 30 and 2750 V, respectively; and the source temperature was 70 °C. For the time-of-flight (TOF) analysis, the scan time was set to 0.5 s in the continuum mode, and the mass range was 50–2000 Da. Human [Glu1] fibrinopeptide B (Sigma-Aldrich) at 100 fmol mm^{-3} was used as an external calibrant, and lock mass acquisition was performed every 30 s. Mass spectrum acquisition was performed over 90 min using MassLynx v.4.0 software (Waters).

2.6. Proteomics data analysis

Spectral processing and comparative analysis were performed using Progenesis QI for Proteomics v. 2 software (Nonlinear Dynamics, Newcastle, UK). The following search parameters were used: 150, 50 and 750 counts for the low-energy, elevated-energy, and intensity thresholds, respectively, one missed cleavage, a minimum of two fragment ions per peptide, a minimum of five fragment ions per protein, a minimum of two peptides per protein, fixed modifications of the carbamidomethyl (C) group and variable modifications of the oxidation (M) and phosphoryl (STY) groups, a default maximum false discovery rate (FDR) of 1%, a peptide score greater than four, and a maximum peptide mass error of 10 ppm. The *C. papaya* protein database in Phytozome V12.1 (https://phytozome.jgi.doe.gov/pz/portal.html) was used for protein identification. The label-free relative quantitative analyses were performed based on the normalized protein ion counts. After the data were processed, only the proteins present in all three runs of the biological replicates were considered. Based on the analysis of variance (ANOVA; $p < 0.05$) results, the differentially abundant proteins were considered upaccumulated if their fold change (FC) was greater than 1.5 and downaccumulated if their FC was lower than 0.667.

Finally, the proteins were functionally characterized using Blast2GO software (www.blast2go.com). Sequences with a biological process not identified by Blast2GO were manually analyzed using the UniProtKB (http://www.uniprot.org/blast/), NCBI (http://www.ncbi.nlm.nih.gov) and Phytozome (https://phytozome.jgi.doe.gov/pz/portal.html#) online BLAST tools. BLAST was performed against the nonredundant (nr) Plants/viridiplantae protein sequences database using the following settings: number of blast hits, 20; blast E-value cut-off, 1.0×10^{-6}; BLAST program, BLASTP; high-scoring segment pair length cut-off, 33; and low complexity filter. The mass spectrometry proteomic data have been deposited in the ProteomeXchange Consortium via the PRIDE (Vizcaino et al., 2016) partner repository with the dataset identifier “PXD009785”.

2.7. Statistical analysis

Light source experiments during embryogenic callus maturation were performed using a completely randomized design. The increment in the FW of the callus and the number of somatic embryos data were analyzed by ANOVA ($p < 0.05$) followed by the Student–Newman–Keuls (SNK) test using R statistical software (R Core Team, 2014).

3. Results

3.1. Effects of light source treatments on the callus fresh weight and number of cotyledonary somatic embryos

Our results showed that the light source significantly affected the development of somatic embryos in the *C. papaya* embryogenic callus (Table 1). At the end of the maturation period, the embryogenic callus matured under the W_mB LED lamp showed a significantly higher number of cotyledonary somatic embryos per callus (82.4) than that matured under the fluorescent lamp (47.6) and other lamps (Table 1). Additionally, the somatic embryos subjected to this treatment were able to undergo phase conversion and ex *vitro* acclimatization, which resulted in the production of normal emblings (Fig. 1G).

The light source also significantly affected the increment in the FW of the *C. papaya* embryogenic callus (Table 1). Based on these results, the embryogenic callus matured under the W_mB LED lamp and that matured under the fluorescent lamp, which is commonly used for *in vitro* cultures, were used to determine the number of somatic embryos at different stages and for proteomic analyses.

In the second experiment, it was possible to observe somatic embryos at the globular (Fig. 1C), heart (Fig. 1D), torpedo (Fig. 1E) and cotyledonary (Fig. 1F) stages under both lamps (Table 2). At the end of the 28-day maturation period, the W_mB LED-treated callus revealed a higher number of cotyledonary embryos than the fluorescent lamp-treated callus (Table 2). At this time point, the fluorescent lamp-treated callus also showed a significantly higher number of globular embryos than the W_mB LED treated callus (Table 2). These findings suggest that the production of cotyledonary embryos might need a longer time with fluorescent lamps than with W_mB LED lamps and highlight the efficiency of the W_mB LED wavelengths in encouraging the maturation of *C. papaya*.

3.2. Effects of W_mB LED and fluorescent lamps on the differential accumulation of proteins during the maturation of papaya somatic embryos

We performed a comparative proteomic analysis of embryogenic callus at 14 days of maturation, which was the point at which most of the somatic embryos were in the globular stage of development, regardless of the treatment. The proteomic analysis identified and quantified a total of 522 proteins, and all the protein and peptide measurements are detailed in Supplementary Tables S2 and S3. We observed 35 differentially accumulated proteins, including 28 up- and 7 downaccumulated proteins, respectively, in the embryogenic callus matured under the W_mB LED lamp compared with that matured under the fluorescent lamp treatment (Table 3). These differentially abundant proteins were functionally classified according to the Gene Ontology biological process category. Among the upaccumulated proteins, the major biological process categories included the transport (6 proteins), carbohydrate metabolic process (5 proteins), cellular response to stimulus (5 proteins), and generation of precursor metabolites and energy (4 proteins) categories (Figs. 2 and 3). For downaccumulated proteins, the carbohydrate metabolic process (3 proteins), cellular response to stimulus (1 protein), and lipid metabolic process (1 protein) were observed (Figs. 2 and 3).

A flowchart summarizing the major proteins and protein groups that showed differential abundance between the embryogenic callus matured under W_mB LED lamp compared with that matured under the fluorescent lamp is presented in Fig. 3.

4. Discussion

4.1. Effects of light source on the maturation of papaya somatic embryos

In our study, higher numbers of cotyledonary somatic embryos were attained with the LED lamp emitting a combination of white and medium-blue wavelengths (W_mB) than with the fluorescent lamp (Tables 1 and 2). Similarly, a previous study showed that LED lamps with the medium-blue wavelength result in the highest number of somatic embryos reaching the maturation phase in the sugarcane embryogenic callus (Heringer et al., 2017). In *V. vinifera*, the highest conversion rate of somatic embryos to normal plantlets was obtained using blue LED light (Tittmann et al., 2015).

It is important to highlight that in our work, only the combination of white and medium-blue wavelengths provided by an LED lamp (W_mB LED) resulted in a significant increase in the number of somatic embryos relative to that attained with fluorescent lamp treatment. The results obtained with the other lamps emitting blue light did not differ significantly from each other or from the results obtained with the fluorescent lamp.

4.2. Effects of W_mB LED and fluorescent lamps on the differential accumulation of proteins during the maturation of papaya somatic embryos

Plants have sophisticated mechanisms to perceive and transduce light stimuli that induce selective changes in the genome, epigenome, transcriptome and proteome. Chromatin compaction resulting from histone modification and DNA methylation is directly impacted by light (Barneche et al., 2014). These stimuli generate different signaling cascades reflected in the proteome profile that promote cell commitment toward embryogenesis.

As our data demonstrated, W_mB LED treatment promotes differentiation of the *C. papaya* embryogenic callus to yield higher numbers of globular and cotyledonary somatic embryos compared with those obtained in the fluorescent lamp-treated embryogenic callus (Table 2). In this sense, we highlight that LED source treatment directly affects the morphogenetic evolution of the embryogenic callus during maturation, which is a process associated with a differential regulation of proteins associated with somatic embryo development. The proteomics analysis

Table 1
Fresh weight and number of cotyledonary somatic embryos, per callus (300 mg of initial FW), of the *C. papaya* 'Golden' embryogenic callus matured under LED lamps emitting different wavelengths and under fluorescent lamp treatments, at 28 days of maturation.

Analysis	Treatment (lamp)						
	Fluorescent	W_hB LED	W_mB LED	W_lB_dR LED	W_mB_dR LED	$W_lB_dR_fR$ LED	$W_mB_dR_fR$ LED
FW (g)	1.63 ab*	1.17b	1.21b	1.70 ab	1.90a	1.45 ab	1.62 ab
Number of somatic embryos	47.6b	42.8b	82.4a	38.6b	41.4b	38.6b	52.8b

*Values followed by the same letter within a row do not differ significantly from each other according to the Student–Newman–Keuls test ($p < 0.05$). LED lamps: W = white, $_l$B = low-blue, $_m$B = medium-blue, $_h$B = high-blue, $_d$R = deep-red, $_f$R = far-red. (n = 5; CV of FW = 21%; CV of number of somatic embryos = 35.9%).

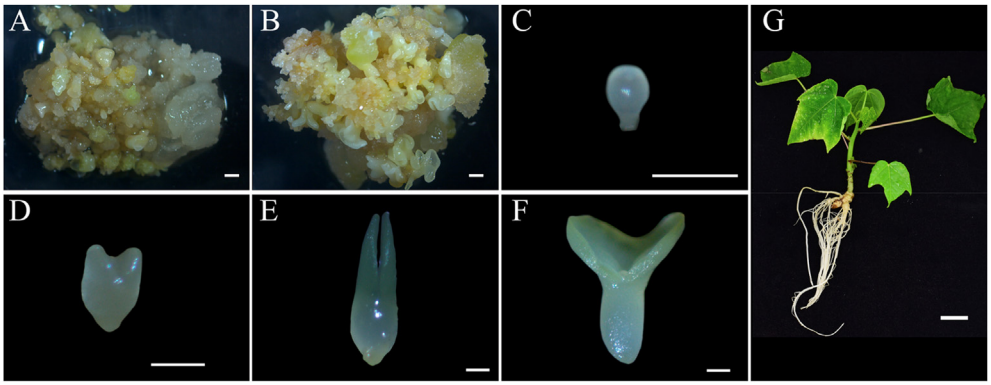

Fig. 1. Embryogenic callus of the *C. papaya* 'Golden' at 28 days of maturation under the fluorescent **(A)** or under the W_mB LED **(B)** lamps. Somatic embryo developmental stages: globular **(C)**, heart **(D)**, torpedo **(E)**, cotyledonary **(F)** and well-regenerated papaya embling (G). Scale bars in (A), (B), and (C) = 0.5 mm. Scale bars in (D), (E), and (F) = 0.1 mm. Scale bar in (G) = 1 cm. (For interpretation of the references to colour in this figure legend, the reader is referred to the Web version of this article.)

Table 2
Number of somatic embryos at the globular, heart, torpedo and cotyledonary stages of the *C. papaya* 'Golden' embryogenic callus matured under the W_mB LED lamp and under the fluorescent lamp.

Embryo stage	W_mB LED		Fluorescent	
	Day 14	Day 28	Day 14	Day 28
Globular	59.28Aa	12.42Bb	44.42Ba	23.00Ab
Heart	7.85Aa	4.28Ab	8.85Aa	3.71Ab
Torpedo	20.28Aa	20.00Aa	17.85Aa	21.28Ab
Cotyledonary	4.71Ab	61.00Aa	5.42Ab	39.57Ba

*Capital letters denote significant differences between the treatments at the same maturation time. Lowercase letters denote significant differences between the culture times within the same treatment. Means followed by different letters are significantly different according to the Student–Newman–Keuls test ($p < 0.05$). ($n = 7$; $CV_{Globular} = 13.7\%$; $CV_{Heart} = 46.3\%$; $CV_{Torpedo} = 21.3\%$; $CV_{Cotyledonary} = 17\%$).

performed in this study showed the presence of differentially abundant proteins between embryogenic callus incubated under the W_mB LED lamp and that incubated under the fluorescent lamp at 14 days of maturation.

Investigation of the biological process functional classification categories of these proteins indicated that the highest numbers of upaccumulated proteins were grouped into the transport (6), carbohydrate metabolic process (5), cellular response to stimulus (5), and generation of precursor metabolites and energy (4) categories (Figs. 2 and 3 and Table 3). These proteins might be related to energy production, cell wall modifications and cellular traffic, which are required for morphogenetic processes during the maturation of somatic embryos, as observed in other studies investigating somatic embryogenesis (Ge et al., 2014; Heringer et al., 2018; Zhao et al., 2015).

The upaccumulated proteins in the *C. papaya* 'Golden' embryogenic callus matured under the W_mB LED lamp compared with that matured under the fluorescent lamp include aconitate hydratase (PACID = 16427747), triosephosphate isomerase (TPI; PACID = 16426898) and alcohol dehydrogenase 1 (ADH1; PACID = 16415822) (Table 3), which are linked to metabolic processes such as the TCA cycle, sucrose pathway, glycolysis and fermentation (Carrari et al., 2003; Henze et al., 1994; Strommer, 2011). Several researchers have suggested that the glycolytic pathway and the TCA cycle are of central importance in somatic embryo development, particularly during the maturation phase (Ge et al., 2014; Xu et al., 2012). The TPI enzyme is essential for effective energy generation (Zhou et al., 2009) and has been associated with the early stages of somatic embryo development in the embryogenic callus of other species (Xu et al., 2012; Zhao et al., 2015). Moreover, ADH activity is positively correlated with the embryogenic capacity in *Bactris gasipaes* (Heringer et al., 2014) and is higher in the *C. papaya* 'UENF/CALIMAN 01' embryogenic callus (Vale et al., 2014). The identification of a wide range of proteins involved in processes of energy metabolism might be linked to the active metabolic demand during somatic embryo development, and these proteins could be associated with the higher number of somatic embryos observed in the embryogenic callus matured under the W_mB LED lamp compared with that matured under the fluorescent lamp treatment.

In our study, the chloroplastic enzymes glyceraldehyde-3-phosphate dehydrogenase (GAPCp; PACID = 16417433) and pyruvate kinase (PK_p; PACID = 16418124) were upaccumulated in embryogenic callus matured under the W_mB LED lamp treatment compared with that matured under the fluorescent lamp treatment (Table 3). In non-photosynthetic cells, GAPCp plays a crucial role in serine biosynthesis and sugar and amino acid metabolism, and this role is linked to abscisic acid signal transduction (Muñoz-Bertomeu et al., 2011). In addition, the PK_p protein participates in fatty acid metabolism during the maturation of *Arabidopsis* zygotic embryos (Baud et al., 2007). Our results indicate the possible participation of both enzymes in primary metabolism at the heterotrophic phases due to their association with the improvements in the development of somatic embryos in the embryogenic callus during maturation under the W_mB LED lamp.

Proteins associated with *in vitro* morphogenesis, such as cell division cycle 48 (CDC48; PACID = 16422729) and actin-depolymerizing factor 2 (ADF2; PACID = 16404304), were upaccumulated in the embryogenic callus matured under the W_mB LED lamp treatment compared with that matured under the fluorescent lamp treatment (Table 3). During somatic embryogenesis, CDC48 colocalizes with a transmembrane somatic embryogenesis receptor-like kinase 1 (SERK1) (Aker et al., 2006), and two CDC48 proteins were highly abundant in cell lines responsive to the development of *Araucaria angustifolia* somatic embryos (dos Santos et al., 2016). The upaccumulation of CDC48 in the *C. papaya* 'Golden' embryogenic callus matured under the W_mB LED lamp might indicate a role for CDC48 in promoting embryogenic development through the regulation of different cellular processes, such as the cell cycle.

Moreover, in response to stress conditions, ADF regulates F-actin organization and dynamics to contribute to cellular growth and development (Tang et al., 2017). During *in vitro* shoot regeneration, the inhibition of *ADF* gene expression disrupts the architecture of microfilaments and thereby affects stem cell initiation and auxin polar transport and distribution (Tang et al., 2017). A transcriptome analysis during early somatic embryogenesis in *Elaeis guineensis* showed an accumulation of *ADF* transcripts (Lin et al., 2009). This information and the data obtained in our study suggest the participation of ADF proteins in cellular polarity, division orientation, cell elongation and auxin polar transport, which results in the enhanced maturation and progression of somatic embryos to the cotyledonary stage in the *C. papaya* 'Golden' embryogenic callus under the W_mB LED lamp at 14 days of maturation.

In addition, the IAA-amido synthetase protein (PACID = 16423668) was upaccumulated in the embryogenic callus matured under the W_mB LED lamp compared with that matured under the fluorescent lamp

Table 3
Differentially accumulated proteins during maturation of the *C. papaya* 'Golden' embryogenic callus under W_mB LED and fluorescent lamps.

PAC ID Phytozome	Protein description	Biological process	Peptide count	Confidence score	Average of normalized total ion count		Anova (p)	Fold change W_mB LED/Fluorescent	W_mB LED/ Fluorescent
					Fluorescent	W_mB LED			
16414912	Polygalacturonase-like	Carbohydrate metabolic process; Cell wall organization	12	88.3	54848.1	213581.8	0.0009	3.8941	UP
16429982	Nuclear pore complex protein NUP50A	Transport	2	11.2	831.2	2544.8	0.0003	3.0616	UP
16409958	CASP-like protein 1D1	Cell wall organization	4	27.1	2825.3	8126.2	0.0011	2.8762	UP
16408289	Glycine cleavage system H-protein 2, mitochondrial-like	Cellular amino acid metabolic process	3	24.1	1408.1	3731.1	0.0288	2.6497	UP
16427022	Ist1-like protein	Protein transport	2	12.0	143.2	343.9	0.0187	2.4014	UP
16413904	GTP-binding YPTM2	Transport; Vesicle-mediated transport; Cell communication	13	86.7	26117.0	61635.5	0.0037	2.3600	UP
16421876	Germin-like protein subfamily 1 member 13	Cell wall organization	2	21.4	7900.6	17121.2	0.0172	2.1671	UP
16406437	Slit homolog 2 protein-like isoform X2	Unknown	2	12.7	6286.7	13335.0	0.0003	2.1212	UP
16425359	Probable alpha-mannosidase At5g13980 isoform X2	Carbohydrate metabolic process	2	18.5	11379.9	24112.3	0.0077	2.1188	UP
16408604	Nucleus-like protein	Unknown	10	65.1	34726.8	70520.6	0.0026	2.0307	UP
16424654	Pollen-specific protein C13-like	Unknown	4	31.1	9204.1	17969.6	0.0057	1.9524	UP
16404304	Actin-depolymerizing factor 2-like	Defense response; Protein depolymerization	4	33.2	27861.1	53132.9	0.0425	1.9071	UP
16420788	Pyrophosphate-energized vacuolar membrane proton pump 1-like	Transport; Generation of precursor metabolites and energy	14	113.6	11983.8	22517.9	0.0144	1.8790	UP
16426898	Triosephosphate isomerase	Carbohydrate metabolic process; Generation of precursor metabolites and energy	10	66.1	19552.2	34532.7	0.0025	1.7662	UP
16405381	ATP-binding protein, putative	Chromosome segregation	5	29.1	1562.0	2712.6	0.0190	1.7366	UP
16426975	Ras-related protein Rab11C	Transport; Cell communication	8	53.2	3321.3	5720.8	0.0058	1.7224	UP
16417433	Glyceraldehyde-3-phosphate dehydrogenase GAPCP2	Carbohydrate metabolic process	7	62.9	12904.6	22200.0	0.0030	1.7203	UP
16422729	Cell division cycle protein 48 homolog	Transport; Cellular component organization or biogenesis; Cell cycle; Cell division	16	125.9	11546.7	19825.6	0.0121	1.7170	UP
16429896	Proteasome subunit alpha type-6	Protein processing; Ubiquitin-dependent protein catabolic process	2	13.7	8714.3	14348.0	0.0237	1.6465	UP
16415822	Alcohol dehydrogenase 1	Cellular response to stimulus; Positive regulation of cellular response to hypoxia; Oxidation reduction process	8	84.6	2736.0	4471.6	0.0220	1.6343	UP
16425047	Glutamate decarboxylase 5	Cellular amino acid metabolic process	5	32.2	3240.9	5257.3	0.0367	1.6222	UP
16409589	PLAT domain-containing protein 3-like	Lipid metabolic process; Oxylipin biosynthetic process	5	48.1	135344.6	217997.9	0.0180	1.6107	UP
16423668	Probable indole-3-acetic acid-amido synthetase GH3.1	Cellular response to stimulus; Response to auxin; Response to light stimulus	34	351.1	1067883.7	1700492.9	0.0129	1.5924	UP
16409223	Hevein-like preproprotein	Defense response	6	42.9	105139.8	166983.5	0.0093	1.5882	UP
16428797	Glycine-rich RNA-binding protein 2, mitochondrial	Cellular response to stimulus; mRNA processing	3	28.9	7639.1	12091.3	0.0145	1.5828	UP
16418124	Pyruvate kinase isozyme A, chloroplastic	Carbohydrate metabolic process; Generation of precursor metabolites and energy; Lipid metabolic process	9	51.8	25090.3	38727.5	0.0201	1.5435	UP
16427747	Aconitate hydratase, cytoplasmic	Generation of precursor metabolites and energy; Cellular respiration	19	153.9	78480.7	121105.9	0.0396	1.5431	UP
16408662	Probable mitochondrial-processing peptidase subunit beta, mitochondrial	Protein processing	6	36.3	23118.1	35408.6	0.0114	1.5316	UP
16429637	Glycoside hydrolase family 1 protein	Carbohydrate metabolic process	11	112.6	19581.0	5612.2	0.0003	0.2866	DOWN
16429727	Myrosinase 4-like	Carbohydrate metabolic process	22	221.4	341674.6	139092.1	0.0052	0.4071	DOWN
16410647	Myrosinase 4-like	Carbohydrate metabolic process	13	127.3	61390.5	31566.5	0.0008	0.5142	DOWN

(*continued on next page*)

Table 3 (*continued*)

PAC ID Phytozome	Protein description	Biological process	Peptide count	Confidence score	Average of normalized total ion count		Anova (p)	Fold change W_mB LED/Fluorescent	W_mB LED/ Fluorescent
					Fluorescent	W_mB LED			
16419850	Peroxidase N1-like	Metabolic process; Cellular process; Response to stimulus; Detoxification	16	121.2	681612.9	383000.5	0.0357	0.5619	DOWN
16415425	Natterin-like protein	Unknown	20	178.2	523763.8	294685.5	0.0040	0.5626	DOWN
16425358	Probable alpha-mannosidase At5g13980	Metabolic process	4	23.5	7023.0	4362.6	0.0212	0.6212	DOWN
16410656	GDSL esterase/lipase At5g45670-like	Lipid metabolic process	18	131.1	113396.5	74763.9	0.0236	0.6593	DOWN

(Table 3). This enzyme acts by conjugating excess active auxin in its inactive form to amino acids, which results in the maintenance of hormonal homeostasis during somatic embryogenesis (Heringer et al., 2018). Thus, the identification of IAA-amido synthetase in the *C. papaya* 'Golden' embryogenic callus and other species (Heringer et al., 2018) might indicate that endogenous free auxin is conjugated and that the hormone levels are decreasing.

The proton-translocating inorganic pyrophosphatase protein (H^+-PPase; PACID = 16420788) was also upaccumulated in the embryogenic callus matured under the W_mB LED lamp compared to that treated under the fluorescent lamp (Table 3). This transporter can acidify the vacuolar lumen and other endomembrane compartments. H^+-PPase appears to be the major H^+ pump in sugarcane embryogenic callus and has an essential role in embryogenic competence acquisition during maturation (Passamani et al., 2018). We observed several differentially accumulated proteins in the embryogenic callus matured under the W_mB LED lamp treatment that are related to developmental processes such as cell cycle control, auxin metabolism and transport as well as ionic homeostasis. The increases in the abundances of these proteins could be associated with the higher differentiation level observed in the embryogenic callus matured under the W_mB LED lamp treatment.

Proteins involved in internal transport, including IST1 (PACID = 16427022), NUP50A (PACID = 16429982) and the Rab proteins RAB-11C (PACID = 16426975) and GTP-binding YPTM2 (PACID = 16413904), were upaccumulated in the embryogenic callus matured under the W_mB LED lamp compared with that matured under the fluorescent lamp (Table 3). The IST1 protein interacts with components of the endosomal sorting complex required for transport (a membrane complex) (Buono et al., 2016). NUP50A is a component of the nuclear pore complex and plays a role in the exchange of RNA and proteins between the nucleus and the cytoplasm via interactions with Rab GTPase proteins (Tamura et al., 2010). The proteins of the Rab GTPase family regulate the transport of vesicles and the *trans*-Golgi network (TGN) (Uemura and Ueda, 2014). The accumulation of proteins involved in transport in the W_mB LED-treated embryogenic callus could be associated with the higher number of globular somatic embryos obtained with this treatment and with a correct internal trafficking of molecules, which would favor normal embryonic development.

Polygalacturonase (PG; PACID = 16414912) and germin-like (GLP; PACID = 16421876) proteins were upaccumulated in the embryogenic callus matured under the W_mB LED lamp compared with that subjected to the fluorescent lamp treatment (Table 3). These two proteins are related to cell wall rearrangement. PG catalyzes the cleavage of pectin polymers and thereby determines cell division, expansion and differentiation (Daher and Braybrook, 2015). GLPs are widely detected during early somatic embryo development in several species and function as structural proteins or receptors during somatic embryogenesis and stress responses (Mahdavi-Darvari et al., 2015). Thus, the accumulation of PG and GLPs in the embryogenic callus matured under the W_mB LED lamp indicates important roles for these proteins in cell wall plasticity, which would allow more efficient maturation of *C. papaya* somatic embryos.

Three of the seven proteins that were downaccumulated in the embryogenic callus matured under the W_mB LED lamp treatment compared with that matured under the fluorescent lamp treatment were myrosinases: one glycoside hydrolase family 1 protein (PACID = 16429637) and two myrosinase 4-like proteins (PACID = 16429727 and PACID = 16410647) (Table 3). These enzymes can generate the products isothiocyanates, epithionitriles, nitriles, and thiocyanates and catalyze the production of indole-3-acetonitrile, which can be hydrolyzed by nitrilases to form auxin (Bhat and Vyas, 2019). This protein was also downaccumulated in the *C. papaya* 'UENF/Caliman 01' embryogenic callus treated with PEG (Vale et al., 2014). These observations highlight the considerable accumulation of this protein family in embryogenic callus incubated under fluorescent

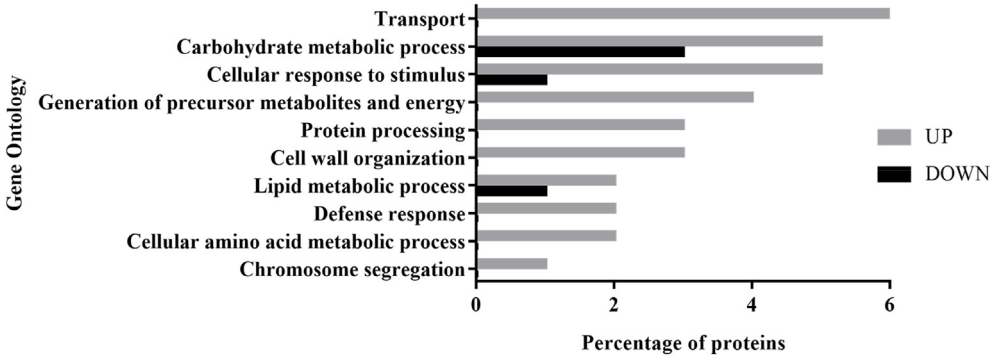

Fig. 2. Functional classification based on the gene ontology of up- and downaccumulated proteins in the *C. papaya* 'Golden' embryogenic callus matured under the W_mB LED lamp compared with that matured under the fluorescent lamp.

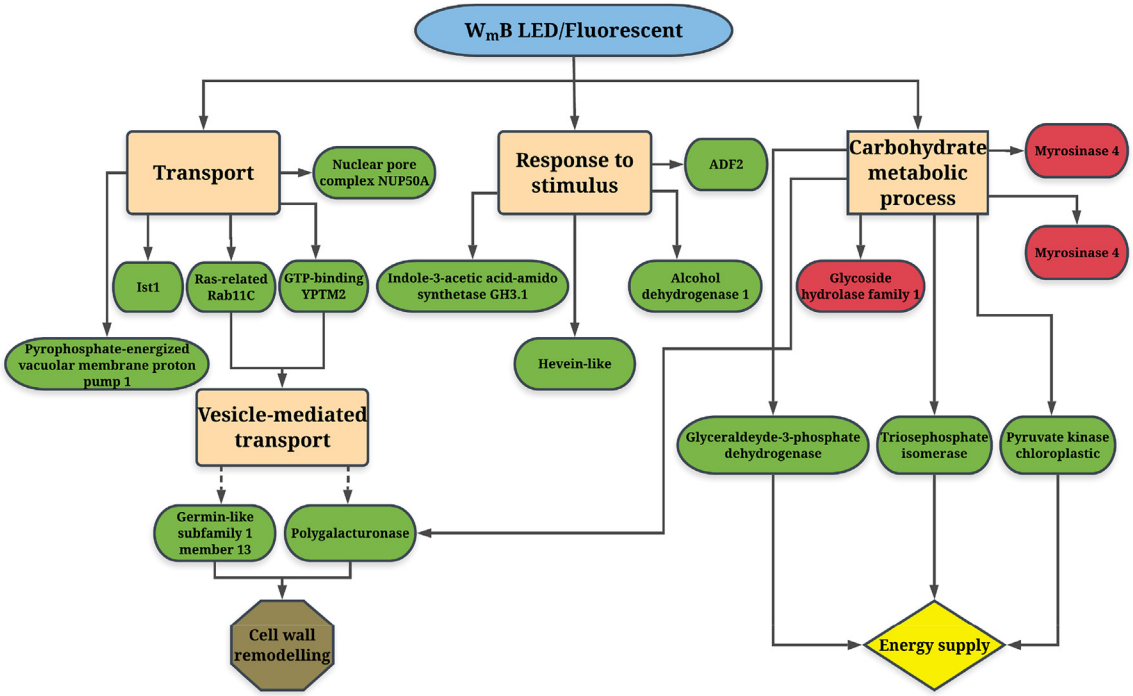

Fig. 3. Flowchart summarizing the major differentially accumulated proteins and their related biological processes in the *C. papaya* 'Golden' embryogenic callus matured under the W_mB LED lamp compared with that matured under the fluorescent lamp. The green boxes indicate the upaccumulated proteins, and the red boxes show the downaccumulated proteins. The beige boxes present the biological processes represented by the proteins, and the brown and yellow boxes show the final cellular responses. (For interpretation of the references to colour in this figure legend, the reader is referred to the Web version of this article.)

lamps, which, at least in part, can disrupt endogenous auxin homeostasis or the accumulation of toxic compounds such as isothiocyanates to interfere with somatic embryo differentiation and development.

5. Conclusion

The use of LED lamps emitting W_mB wavelengths for maturation of the *C. papaya* 'Golden' embryogenic callus shows great potential as a replacement for the use of conventional fluorescent lamps, because these lamps significantly increase the number of mature somatic embryos, and these findings provide support for the optimization of protocols for somatic embryogenesis in this species. *C. papaya* 'Golden' embryogenic callus at 14 days of maturation under the W_mB LED compared with that matured under the fluorescent lamps showed a differential accumulation of proteins. The morphogenetic evolution of the embryogenic callus during maturation under W_mB LED lamp treatment is associated with the upaccumulation of proteins related to energy metabolism (aconitate, ADH1, and TPI), cytoskeletal organization (ADF2) and cell wall remodeling (PG and GLPs) in the maturing embryogenic callus, which can enhance the functional cellular machinery necessary for further embryo development during maturation. Moreover, important proteins related to auxin homeostasis (GH3) and the normal polar distribution of auxins (ADF2 and IST1) were identified, which suggests that the increases in their accumulation in the embryogenic callus under the W_mB LED lamp treatment might have facilitated the establishment of correct embryo symmetry. The functional trafficking among vacuoles, endosomes, TGN and the nucleocytoplasmic region aided by small GTPase proteins and nucleoporin NUP50A can be essential for somatic embryo development by promoting active molecular transport through cells and leading to the enhanced maturation obtained under the W_mB LED lamp treatment compared with the fluorescent lamp treatment.

Author contributions

VS, FA and CSC contributed to the conception and design of the

study; FA and EV performed the somatic embryo maturation experiments; FA and RR performed the proteomics analysis; FA wrote the first draft of the manuscript; and VS, CSC and FA wrote sections of the manuscript. All the authors contributed to the revision of the manuscript and read and approved the submitted version of the manuscript.

Funding

This research was funded by the Carlos Chagas Filho Foundation for Research Support in the State of Rio de Janeiro (FAPERJ) (Proc. E26/211.690/2015; Proc. E26/203.311/2017) and the National Council for Scientific and Technological Development-CNPq (305415/2016-6) to VS. This study was financed in part by the Coordenação de Aperfeiçoamento de Pessoal de Nível Superior - Brasil (CAPES) - Finance Code 001.

Conflicts of interest

The authors declare that this study was conducted in the absence of any commercial or financial relationships that could be construed as a potential conflict of interest.

Acknowledgments

We would like to thank the Coordination for the Improvement of Higher Education Personnel (CAPES) and FAPERJ for the graduate scholarships provided to FAA and RSR, respectively. We kindly thank Caliman Agrícola S/A for supplying the fruits.

Appendix A. Supplementary data

Supplementary data to this article can be found online at https://doi.org/10.1016/j.plaphy.2019.08.029.

References

Aker, J., Borst, J.W., Karlova, R., de Vries, S., 2006. The *Arabidopsis thaliana* AAA protein CDC48A interacts in vivo with the somatic embryogenesis receptor-like kinase 1 receptor at the plasma membrane. J. Struct. Biol. 156 (1), 62–71. https://doi.org/10.1105/tpc.105.039412.

Barneche, F., Malapeira, J., Mas, P., 2014. The impact of chromatin dynamics on plant light responses and circadian clock function. J. Exp. Bot. 65 (11), 2895–2913. https://doi.org/10.1093/jxb/eru011.

Baud, S., Wuillème, S., Dubreucq, B., De Almeida, A., Vuagnat, C., Lepiniec, L., et al., 2007. Function of plastidial pyruvate kinases in seeds of *Arabidopsis thaliana*. Plant J. 52 (3), 405–419. https://doi.org/10.1111/j.1365-313X.2007.03232.x.

Bhat, R., Vyas, D., 2019. Myrosinase: insights on structural, catalytic, regulatory, and environmental interactions. Crit. Rev. Biotechnol. 39 (4), 508–523. https://doi.org/10.1080/07388551.2019.1576024.

Bhattacharya, J., Khuspe, S., 2001. In vitro and in vivo germination of papaya (*Carica papaya* L.) seeds. Sci. Hortic. 91 (1), 39–49. https://doi.org/10.1016/s0304-4238(01)00237-0.

Buono, R.A., Paez-Valencia, J., Miller, N.D., Goodman, K., Spitzer, C., Spalding, E.P., et al., 2016. Role of SKD1 regulators LIP5 and IST1-LIKE1 in endosomal sorting and plant development. Plant Physiol.. 171 (1), 251–264. https://doi.org/10.1104/pp.16.00240.

Carrari, F., Nunes-Nesi, A., Gibon, Y., Lytovchenko, A., Loureiro, M.E., Fernie, A.R., 2003. Reduced expression of aconitase results in an enhanced rate of photosynthesis and marked shifts in carbon partitioning in illuminated leaves of wild species tomato. Plant Physiol.. 133 (3), 1322–1335. https://doi.org/10.1104/pp.103.026716.

Cheng, Y.L., Tu, S.L., 2018. Alternative splicing and cross-talk with light signaling. Plant Cell Physiol. 59 (6), 1104–1110. https://doi.org/10.1093/pcp/pcy089.

Daher, F.B., Braybrook, S.A., 2015. How to let go: pectin and plant cell adhesion. Front. Plant Sci. 6, 523. https://doi.org/10.3389/fpls.2015.00523.

Dhekney, S., Kandel, R., Bergey, D., Sitther, V., Soorianathasundaram, K., Litz, R., 2016. Advances in papaya biotechnology. Biocatal. Agric. Biotechnol. 5, 133–142. https://doi.org/10.1016/j.bcab.2016.01.004.

dos Santos, A.L.W., Elbl, P., Navarro, B.V., de Oliveira, L.F., Salvato, F., Balbuena, T.S., et al., 2016. Quantitative proteomic analysis of *Araucaria angustifolia* (Bertol.) Kuntze cell lines with contrasting embryogenic potential. J. Proteom. 130, 180–189. https://doi.org/10.1016/j.jprot.2015.09.027.

Fabi, J.P., Cordenunsi, B.R., de Mattos Barreto, G.P., Mercadante, A.Z., Lajolo, F.M., Oliveira do Nascimento, J.R., 2007. Papaya fruit ripening: response to ethylene and 1-methylcyclopropene (1-MCP). J. Agric. Food Chem. 55 (15), 6118–6123. https://doi.org/10.1021/jf070903c.

Fehér, A., 2015. Somatic embryogenesis—stress-induced remodeling of plant cell fate. Biochim. Biophys. Acta 1849 (4), 385–402. https://doi.org/10.1016/j.bbagrm.2014.07.005.

Ge, X., Zhang, C., Wang, Q., Yang, Z., Wang, Y., Zhang, X., et al., 2014. iTRAQ protein profile differential analysis between somatic globular and cotyledonary embryos reveals stress, hormone, and respiration involved in increasing plantlet regeneration of *Gossypium hirsutum* L. J. Proteome Res. 14 (1), 268–278. https://doi.org/10.1021/pr500688g.

Gupta, S.D., Jatothu, B., 2013. Fundamentals and applications of light-emitting diodes (LEDs) in *in vitro* plant growth and morphogenesis. Plant Biotechnol. Rep. 7 (3), 211–220. https://doi.org/10.1007/s11816-013-0277-0.

Henze, K., Schnarrenberger, C., Kellermann, J., Martin, W., 1994. Chloroplast and cytosolic triosephosphate isomerases from spinach: purification, microsequencing and cDNA cloning of the chloroplast enzyme. Plant Mol. Biol. 26 (6), 1961–1973. https://doi.org/10.1007/BF00019506.

Heringer, A.S., Reis, R.S., Passamani, L.Z., de Souza-Filho, G.A., Santa-Catarina, C., Silveira, V., 2017. Comparative proteomics analysis of the effect of combined red and blue lights on sugarcane somatic embryogenesis. Acta Physiol. Plant. 39 (2), 52. https://doi.org/10.1007/s11738-017-2349-1.

Heringer, A.S., Santa-Catarina, C., Silveira, V., 2018. Insights from proteomic studies into plant somatic embryogenesis. Proteomics 18 (5–6), 1700265. https://doi.org/10.1002/pmic.201700265.

Heringer, A.S., Steinmacher, D.A., Fraga, H.P., Vieira, L.N., Montagna, T., Quinga, L.A., et al., 2014. Improved high-efficiency protocol for somatic embryogenesis in Peach Palm (*Bactris gasipaes* Kunth) using RITA® temporary immersion system. Sci. Hortic. 179, 284–292. https://doi.org/10.1016/j.scienta.2014.09.041.

Li, H., Lin, Y., Chen, X., Bai, Y., Wang, C., Xu, X., et al., 2018. Effects of blue light on flavonoid accumulation linked to the expression of miR393, miR394 and miR395 in longan embryogenic calli. PLoS One 13 (1), e0191444. https://doi.org/10.1371/journal.pone.0191444.

Lin, H.-C., Morcillo, F., Dussert, S., Tranchant-Dubreuil, C., Tregear, J.W., Tranbarger, T.J., 2009. Transcriptome analysis during somatic embryogenesis of the tropical monocot *Elaeis guineensis*: evidence for conserved gene functions in early development. Plant Mol. Biol. 70 (1–2), 173–192. https://doi.org/10.1007/s11103-009-9464-3.

Mahdavi-Darvari, F., Noor, N.M., Ismanizan, I., 2015. Epigenetic regulation and gene markers as signals of early somatic embryogenesis. Plant Cell Tissue Organ Cult. 120 (2), 407–422. https://doi.org/10.1007/s11240-014-0615-0.

Muñoz-Bertomeu, J., Anoman, A.D., Toujani, W., Cascales-Miñana, B., Flores-Tornero, M., Ros, R., 2011. Interactions between abscisic acid and plastidial glycolysis in *Arabidopsis*. Plant Signal. Behav. 6 (1), 157–159. https://doi.org/10.4161/psb.6.1.14312.

Murashige, T., Skoog, F., 1962. A revised medium for rapid growth and bio assays with tobacco tissue cultures. Physiol. Plant. 15 (3), 473–497. https://doi.org/10.1111/j.1399-3054.1962.tb08052.x.

Nanjo, Y., Skultety, L., Uváčková, L., Klubicová, K., Hajduch, M., Komatsu, S., 2012. Mass spectrometry-based analysis of proteomic changes in the root tips of flooded soybean seedlings. J. Proteome Res. 11 (1), 372–385.

Passamani, L.Z., Bertolazi, A.A., Ramos, A.C., Santa-Catarina, C., Thelen, J.J., Silveira, V., 2018. Embryogenic competence acquisition in sugarcane callus is associated with differential H^+ pump abundance and activity. J. Proteome Res. https://doi.org/10.1021/acs.jproteome.8b00213.

Pasternak, T., Dudits, D., 2019. Epigenetic clues to better understanding of the asexual embryogenesis in planta and in vitro. Front. Plant Sci. 10 (778). https://doi.org/10.3389/fpls.2019.00778.

R Core Team, 2014. R: a Language and Environment for Statistical Computing. R Foundation for Statistical Computing, Vienna, Austria.

Sánchez-Retuerta, C., Suaréz-López, P., Henriques, R., 2018. Under a new light: regulation of light-dependent pathways by non-coding RNAs. Front. Plant Sci. 9, 962. https://doi.org/10.3389/fpls.2018.00962.

Strommer, J., 2011. The plant ADH gene family. Plant J. 66 (1), 128–142. https://doi.org/10.1111/j.1365-313X.2010.04458.x.

Tamura, K., Fukao, Y., Iwamoto, M., Haraguchi, T., Hara-Nishimura, I., 2010. Identification and characterization of nuclear pore complex components in *Arabidopsis thaliana*. Plant Cell Online 22 (12), 4084–4097. https://doi.org/10.1105/tpc.110.079947.

Tang, L.P., Li, X.M., Dong, Y.X., Zhang, X.S., Su, Y.H., 2017. Microfilament depolymerization is a pre-requisite for stem cell formation during *in vitro* shoot regeneration in *Arabidopsis*. Front. Plant Sci. 8, 158. https://doi.org/10.3389/fpls.2017.00158.

Tittmann, S., Borner, M., Harst, M., Bleser, E., 2015. Influence of led-illumination to the regeneration potential of somatic embryos of *Vitis vinifera* 'Chardonnay' - preliminary studies. Acta Hortic. (Wagening.) 1083, 445–453. https://doi.org/10.17660/ActaHortic.2015.1083.57.

Uemura, T., Ueda, T., 2014. Plant vacuolar trafficking driven by RAB and SNARE proteins. Curr. Opin. Plant Biol. 22, 116–121. https://doi.org/10.1016/j.pbi.2014.10.002.

Vale, E., Heringer, A.S., Barroso, T., da Silva Ferreira, A.T., da Costa, M.N., Perales, J.E.A., et al., 2014. Comparative proteomic analysis of somatic embryo maturation in *Carica papaya L.* Proteome Sci. 12 (1), 37. https://doi.org/10.1186/1477-5956-12-37.

Vale, E.M., Reis, R.S., Passamani, L.Z., Santa-Catarina, C., Silveira, V., 2018. Morphological analyses and variation in carbohydrate content during the maturation of somatic embryos of *Carica papaya*. Physiol. Mol. Biol. Plants 1–11. https://doi.org/10.1007/s12298-017-0501-4.

Vizcaino, J.A., Csordas, A., del-Toro, N., Dianes, J.A., Griss, J., Lavidas, I., et al., 2016. 2016 update of the PRIDE database and its related tools. Nucleic Acids Res. 44 (D1), D447–D456. https://doi.org/10.1093/nar/gkv1145.

Wang, Q., Liu, Q., Wang, X., Zuo, Z., Oka, Y., Lin, C., 2018. New insights into the mechanisms of phytochrome–cryptochrome coaction. New Phytol. 217 (2), 547–551. https://doi.org/10.1111/nph.14886.

Xu, H., Zhang, W., Gao, Y., Zhao, Y., Guo, L., Wang, J., 2012. Proteomic analysis of embryo development in rice (*Oryza sativa*). Planta 235 (4), 687–701. https://doi.org/10.1007/s00425-011-1535-4.

Zhao, J., Wang, B., Wang, X., Zhang, Y., Dong, M., Zhang, J., 2015. iTRAQ-based comparative proteomic analysis of embryogenic and non-embryogenic tissues of Prince Rupprecht's larch (*Larix principis-rupprechtii* Mayr). Plant Cell Tissue Organ Cult. 120 (2), 655–669.

Zhou, S., Sauve, R., Thannhauser, T.W., 2009. Aluminum induced proteome changes in tomato cotyledons. Plant Signal. Behav. 4 (8), 769–772. https://doi.org/10.1093/jxb/erp065.